

Intrinsic thermalization of the honeycomb optical latticeA. D. Barr,¹ W. A. Furman¹, M. D. Porter,² and L. E. Reichl¹¹*Center for Complex Quantum Systems and Department of Physics, The University of Texas at Austin, Austin, Texas 78712, USA*²*Sandia National Laboratories, Albuquerque, New Mexico 87185, USA* (Received 19 January 2023; accepted 7 April 2023; published 24 April 2023; corrected 27 April 2023)

Ultracold atoms confined to optical lattices provide a platform for simulation of phenomena not readily accessible in condensed matter and chemical systems. One area of growing interest is the mechanism by which isolated condensed matter systems can thermalize. The mechanism for thermalization of quantum systems has been directly linked to a transition to chaos in their classical counterpart. Here we show that the broken spatial symmetries of the honeycomb optical lattice leads to a transition to chaos in the single-particle dynamics which, in turn, causes mixing of the energy bands of the quantum honeycomb lattice. For systems with single-particle chaos, “soft” interactions between atoms can cause the system to thermalize (achieve a Fermi-Dirac distribution for fermions or a Bose-Einstein distribution for bosons).

DOI: [10.1103/PhysRevE.107.044213](https://doi.org/10.1103/PhysRevE.107.044213)**I. INTRODUCTION**

Ultracold atoms confined to optical lattices provide a platform to explore a variety of phenomena currently inaccessible in condensed matter systems [1,2]. Optical lattices are typically formed by the interference of multiple laser beams. This gives a controllable periodic light structure that is then used to mimic the crystal lattice of a solid. Optical lattices are easily controlled and techniques exist which allow detection of the dynamics of individual atoms in the lattice. These systems can be isolated from outside influences and, in addition to other interesting phenomena, provide a means to study the dynamical mechanisms by which they can thermalize.

The thermalization of an isolated quantum gas of interacting hard sphere particles occurs because the dynamics of the classical counterpart of the system is chaotic. Such systems have spectra whose statistical properties are similar to the spectra of random matrices and they extremize information. When the classical counterpart is chaotic, isolated dilute quantum gases have been shown to have reduced single-particle distribution functions that are Bose-Einstein distributions if the particles are bosons, and Fermi-Dirac distributions if the particles are fermions [3].

The dynamics of isolated noninteracting particles can also become chaotic when the spatial symmetry of the potential energy that confines them is broken. Two classic examples are the dynamics of single particles in the Sinai billiard or the Bunimovitch billiard [4,5]. These billiards induce K-flow in the single-particle dynamics. It has been shown [6–8] that when a gas, with “soft” interactions (interactions that do not induce K-flow), is confined to billiards with single-particle K-flow, the gas can thermalize and have single-particle distributions that are Fermi-Dirac, Bose-Einstein, or even Bose-Einstein condensate (BEC) thermal distributions. This thermalization does not occur in billiards that do not induce K-flow in the single-particle dynamics.

In the sections below, we examine the dynamics of noninteracting ultracold alkali atoms confined to a honeycomb

optical lattice. Honeycomb-like optical lattices have been realized in the laboratory [9]. The honeycomb lattice has been of huge interest to a wide variety of scientists because it has the unique property that there are energy regimes, near the K-points (Dirac points), where the particles become effectively massless (with photon-like dispersion relations). Honeycomb lattices occur naturally in the form of graphene sheets and carbon nanotubes and support the propagation of electron matter waves [10,11]. Honeycomb structures have also been formed with photonic crystals and support interesting electromagnetic wave propagation [12–14].

In Sec. II and Appendix A, we obtain the honeycomb optical lattice considered in subsequent sections. Then in Sec. III, we examine the classical dynamics of the alkali atoms in the optical lattice. In Sec. IV, we examine the quantum dynamics of alkali atoms in the optical lattice, and obtain the energy band structure for the alkali atoms. Finally, in Sec. V, we make some concluding remarks.

II. INTERACTION OF ATOMS WITH OPTICAL LATTICE

We consider noninteracting alkali atoms, with mass m and electric dipole moment d , confined to a honeycomb optical lattice. The optical lattice is created by careful orientation of a system of lasers and oscillating electric fields. The laser radiation interacts with a two-level subsystem of the atom’s electronic levels [15–18]. When the radiation is detuned from resonance with the two-level subsystem, the absorption and emission of radiation exerts a force on the atoms without exciting them. As we show in Appendix A, the Hamiltonian for the alkali atoms in the optical lattice, in Cartesian coordinates, can be written

$$H_{\text{tot}} = \frac{p_x^2}{2m} + \frac{p_z^2}{2m} + 2U + 2U \cos\left[\frac{2k_L x}{\sqrt{3}}\right] - 4U \cos\left[\frac{k_L x}{\sqrt{3}}\right] \cos[k_L z] = E_{\text{tot}}, \quad (1)$$

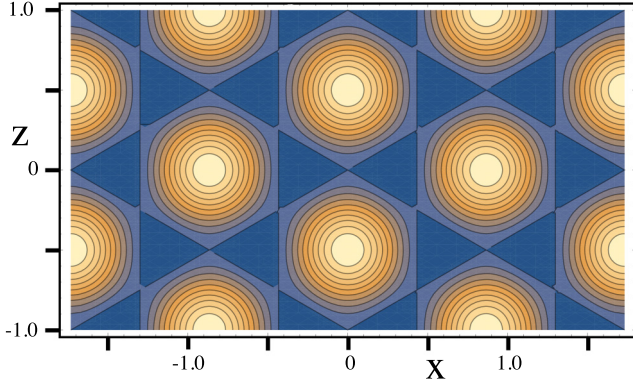


FIG. 1. The honeycomb potential $V(x, z)$ for $U_o = 20$. Along the line $z = 0$, a potential energy minimum occurs for $V(\frac{1}{2\sqrt{3}}, 0) = -20$, a saddle point occurs for $V(0, 0) = 0$, and a potential energy maximum occurs for $V(\frac{\sqrt{3}}{2}, 0) = 160$.

where the wave vector $k_L = \frac{2\pi}{a}$ ($a = \lambda_L$ is the laser wavelength and the lattice constant), $U = \frac{d^2|E_o|^2}{2\hbar\Delta}$, \hbar is Planck's constant, Δ is the detuning of the laser frequency from resonance with the atom, and E_o is the electric field strength.

We now go to dimensionless units. First introduce the energy $E_L = \frac{\hbar^2 k_L^2}{2m}$. Then let $x' = x/a$, $z' = z/a$, $H_{\text{tot}} = H'_{\text{tot}} E_L$, $U = U_o E_L$, $p_x = \hbar k_L p'_x$, and $p_z = \hbar k_L p'_z$. If we substitute these expressions into Eq. (1), divide by E_L , and then drop the primes, we obtain

$$H_{\text{tot}} = p_x^2 + p_z^2 + V(x, z) = E_{\text{tot}}, \quad (2)$$

where

$$V(x, z) = +2U_o + 2U_o \cos\left[\frac{4\pi x}{\sqrt{3}}\right] - 4U_o \cos\left[\frac{2\pi x}{\sqrt{3}}\right] \cos[2\pi z] \quad (3)$$

and E_{tot} is the total energy of the atoms trapped in the optical lattice. Values for various parameters, for the case of cesium atoms in the optical lattice, are given in Appendix B. In the subsequent discussion, we will take $U_o = 20$. A plot of the honeycomb potential $V(x, z)$ for $U_o = 20$ is shown in Fig. 1.

III. CLASSICAL DYNAMICS OF ATOMS IN THE HONEYCOMB OPTICAL LATTICE

The optical lattice Hamiltonian, in Cartesian coordinates, is given by Eqs. (2) and (3). In Fig. 2, we show a unit cell of the classical honeycomb lattice (the region enclosed by the dotted lines). Classically, the energy regime $-20 \leq E_{\text{tot}} \leq 0$ (the dark triangle regions in Fig. 2 is close to integrable, while the energy regime $0 \leq E_{\text{tot}} \leq 160$ (outside the dark triangle in the unit cell) consists of a periodic array of triple peak scatterers (a soft version of the triple hard-disk system [19,20]) which induce completely chaotic behavior (K-flow) in the particle dynamics for a wide range of energies above $E_{\text{tot}} = 0$. For energies closer to the peak at $E = 160$, the particle dynamics begins to show mixed behavior [16,21]. As we shall show below, we find similar behavior for the honeycomb lattice, which for energies $E > 0$ consists of a periodic array of triple peak scatterers.

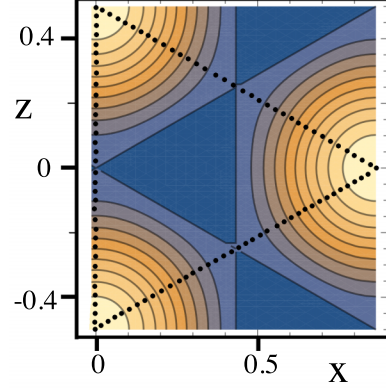


FIG. 2. The unit cell for the classical dynamics is the triangle enclosed by the dark dotted lines. The dotted line runs through three saddle points and three peaks of the potential. The dark triangle in the center is the region with energy $E_{\text{tot}} < 0$. The regions outside the dark inner triangle have energy $0 \leq E_{\text{tot}} \leq 160$.

A. Classical dynamics for $-20 \leq E_{\text{tot}} \leq 0$

In order to show the nature of the particle dynamics for energies $-20 \leq E_{\text{tot}} \leq 0$, it is useful to perform a canonical transformation on the Hamiltonian [Eqs. (2) and (3)]. If we consider the (pendulum-like) Hamiltonian

$$H_x^0 = p_x^2 + 2U_o \cos\left[\frac{4\pi x}{\sqrt{3}}\right] = E_x^0, \quad (4)$$

we can perform a canonical transformation [22] from Cartesian variables (p_x, x) to action-angle variables (J_x, Θ) such that $H_x^0 = E_x^0(J_x)$,

$$x = \frac{\sqrt{3}}{2\pi} \sin^{-1}\left[k \operatorname{sn}\left(\frac{32}{3\pi} \mathbf{K}(k)\Theta, k\right)\right] + \frac{\sqrt{3}}{4}, \quad (5)$$

and

$$p_x = 2k \sqrt{U_o} \operatorname{cn}\left(\frac{32}{3\pi} \mathbf{K}(k)\Theta, k\right), \quad (6)$$

where the modulus $k^2 = \frac{E_x(J_x) + 2U_o}{4U_o}$ (note that $0 \leq k \leq 1$). For $U_o = 20$, the condition $0 \leq k \leq 1$ requires $-40 \leq E_x \leq +40$ and $0 \leq J_x \leq 8.3$. Since the action is quantized in units of Planck's constant, we expect there will be no more than eight quantum states for $E_{\text{tot}} < 0$ [23].

In terms of (J_x, Θ, p_z, z) , the total Hamiltonian takes the form

$$H_{\text{tot}} = E_x^0(J_x) + p_z^2 + 4U_o k \operatorname{sn}\left(\frac{32}{3\pi} \mathbf{K}(k)\Theta, k\right) \cos[2\pi z] + 2U_o = E_{\text{tot}}. \quad (7)$$

The nature of the dynamics becomes clear if we note the series expansion for the Jacobi sn function $\operatorname{sn}\left[\frac{32}{3\pi} \mathbf{K}(k)\Theta, k\right] = \sum_{\ell=0}^{\infty} C_{\ell}(k) \sin[(2\ell + 1)\frac{16}{3}\Theta]$, where $C_{\ell}(k) = \frac{\pi}{k\mathbf{K}(k)} \operatorname{csch}\left[(2\ell + 1)\frac{\pi}{2} \frac{\mathbf{K}(k')}{\mathbf{K}(k)}\right]$. Some values of $C_{\ell}(k)$ include $C_0(0.999999) = 1.2530$, $C_0(0.5) = 1.0176$, $C_0(0.1) = 1.00063$, $C_1(0.999999) = 0.3687$, $C_1(0.5) = 0.0180$, $C_1(0.1) = 0.0006$, $C_2(0.999999) = 0.1546$, $C_2(0.5) = 0.0003$, $C_2(0.1) = 4 \times 10^{-7}$. The values of $C_{\ell}(k)$ fall off rapidly with increasing ℓ .

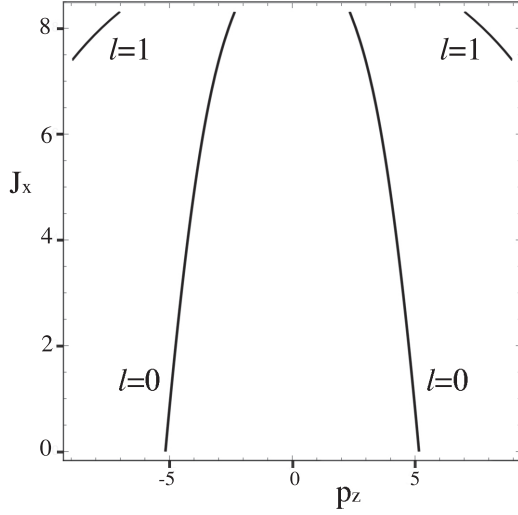


FIG. 3. The Arnold web of resonances for energy $-20 \leq E \leq 0$. The two central resonance lines are $\ell = 0$. The two outer resonance lines are $\ell = 1$.

In terms of the series expansion, the total Hamiltonian takes the form

$$H_{\text{tot}} = E_x^0(J_x) + p_z^2 + 2U_o + 4U_o k \sum_{\ell=0}^{\infty} C_{\ell}(k) \sin \left[(2\ell + 1) \frac{16}{3} \Theta \right] \cos[2\pi z], \quad (8)$$

or

$$H_{\text{tot}} = E_x^0(J) + p_z^2 + 2U_o + \sum_{\ell=0}^{\infty} \left(U_{\ell}(J) \sin \left[(2\ell + 1) \frac{16}{3} \Theta - 2\pi z \right] + U_{\ell}(J) \sin \left[(2\ell + 1) \frac{16}{3} \Theta + 2\pi z \right] \right), \quad (9)$$

where $U_{\ell}(J_x) = \frac{4\pi U_o}{K(k)} \text{csch}[(2\ell + 1) \frac{\pi}{2} \frac{K(k')}{K(k)}]$. Equation (9) shows, explicitly, the resonance structure that governs the dynamics for the energy region $-20 \leq E \leq 0$.

Walker-Ford Hamiltonians

We can now write a Walker-Ford-type Hamiltonian [22,24] for each resonance and examine its impact on the dynamics. The two Hamiltonians that result from the ℓ th term in the series expansion in Eq. (9) can be written

$$H_{\ell}^{\pm} = E_x^0(J_x) + p_z^2 + 2U_o + U_{\ell}(J_x) \sin \left[(2\ell + 1) \frac{16}{3} \Theta \pm 2\pi z \right]. \quad (10)$$

The resonance condition is

$$\left((2\ell + 1) \frac{16}{3} \dot{\Theta} \pm \frac{2\pi \dot{z}}{a} \right) \approx \left((2\ell + 1) \frac{16}{3} \frac{\partial E_x}{\partial J_x} \pm \frac{2\pi p_z}{ma} \right) \ll U_{\ell}(J_x). \quad (11)$$

The location of the resonances as a function of J_x and p_z are plotted in Fig. 3 [22,25,26], which shows the Arnold Web of resonances that contribute to the dynamics for

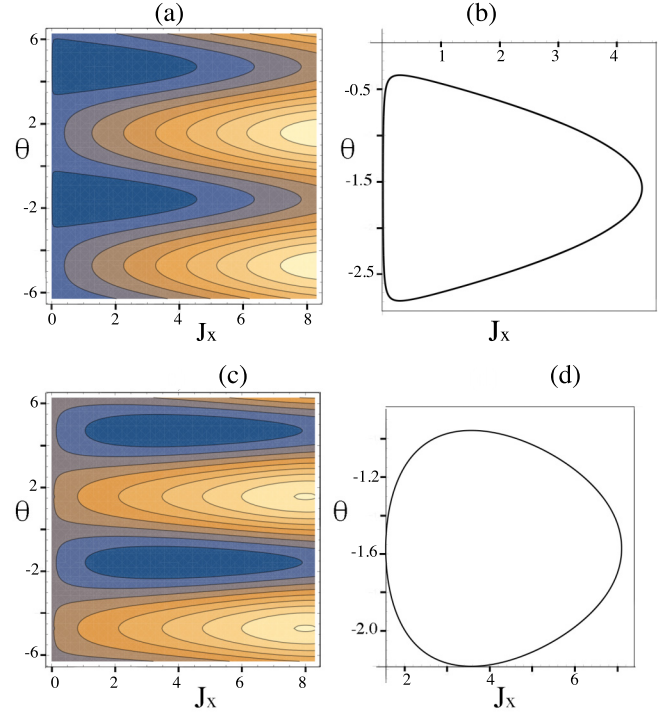


FIG. 4. (a) A plot of total energy E_0^- for the Walker-Ford Hamiltonian ($\ell = 0$) with $I = 6.7$. The dark regions have energy $E_0^- < 0$. (b) A trajectory with $E_0^- = -1.22$. (c) A plot of total energy E_0^- for the Walker-Ford Hamiltonian ($\ell = 0$) with $I = 30.15$. The dark regions have energy $E_0^- < 0$. (d) A trajectory with $E_0^- = -5.99$.

$-20 \leq E_{\text{tot}} \leq 0$. Only the terms for $\ell = 0$ and $\ell = 1$ contribute resonance lines in this energy regime, and these resonance lines do not overlap. This shows that the particle dynamics for $-20 \leq E_{\text{tot}} \leq 0$ is predominantly integrable.

Systems whose dynamics is governed by the Hamiltonian in Eq. (10) have a second constant of the motion, $I_{\ell}^{\pm} = 2\pi J_x \mp (2\ell + 1) \frac{16}{3} p_z$, since one can show that $\frac{dI_{\ell}^{\pm}}{dt} = 0$. We can now write the “resonance” Hamiltonian in the form

$$H_{\ell}^{-} = E_x^0(J_x) + \frac{1}{(2\ell + 1)^2} \left(\frac{3}{16} I_{\ell}^{\pm} - \frac{3\pi}{8} J_x \right)^2 + U_{\ell}(J_x) \sin[\theta] = E_{\ell}^{\pm}, \quad (12)$$

where $\theta = (2\ell + 1) \frac{16}{3} \Theta \mp \frac{2\pi z}{a}$. Equation (12) is the Walker-Ford Hamiltonian. In Fig. 4(a), we plot the total energy E_0^- for the Walker-Ford Hamiltonian for the case $\ell = 0$ and with constant of the motion $I_0^- = 6.7$. In Fig. 4(c), we plot the total energy E_0^- for the Walker-Ford Hamiltonian for the case with constant of the motion $I_0^- = 30.16$. The action variable J_x ranges over the interval $0 < J_x \leq 7$ in Fig. 4(d). Since the action variable is quantized in units of Planck’s constant h [23], we expect that the quantized dynamics can support six to eight quantum states for energies $E_{\text{tot}} < 0$. As we shall see below, it supports six quantum states.

In Fig. 5, we show strobe plots for the exact classical dynamics for $E < 0$. The particle dynamics is dominated by KAM (Kolmogorov-Arnold-Moser) tori [27–29] for energies well below the saddle at $E = 0$. Closer to the saddle the effect of higher order resonance begins to be felt [22].

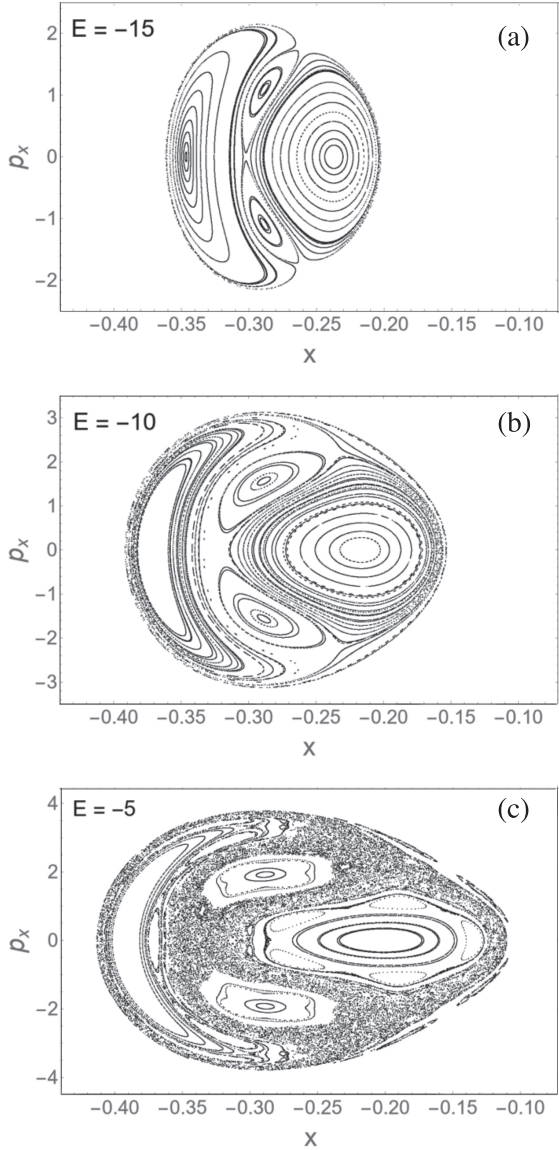


FIG. 5. Surfaces of section (p_x versus x plotted each time $z = 0$ for $p_z > 0$) for energies (a) $E = -15$, (b) $E = -10$, and (c) $E = -5$.

B. Classical dynamics for $E_{\text{tot}} \geq 0$

For energies $0 < E_{\text{tot}} < \infty$, the classical particle dynamics is governed by a lattice composed of a periodic array of a triple Gaussian scattering systems. The triple Gaussian scattering system is a soft version of the classic triple hard-disk scattering system [19,20]. The scattering dynamics of three hard disks is chaotic (a K-flow) at all energies. The soft version of the triple hard-disk potential has been studied in detail in Refs. [16,21], and it has been shown that there is an energy interval below the potential peak where the motion is completely chaotic. Similar behavior was observed in Ref. [16] for a honeycomb lattice composed of Gaussian peaks.

As we show in more detail in Fig. 6, there is a large energy interval ($20 < E < 100$) for which the particle dynamics in the honeycomb optical lattice is a K-flow. Above energies $E > 100$, resonance structures begin to emerge in the classical phase space. As was shown in Ref. [16], these structures can begin to support fairly long-lived, high-energy, quasibound

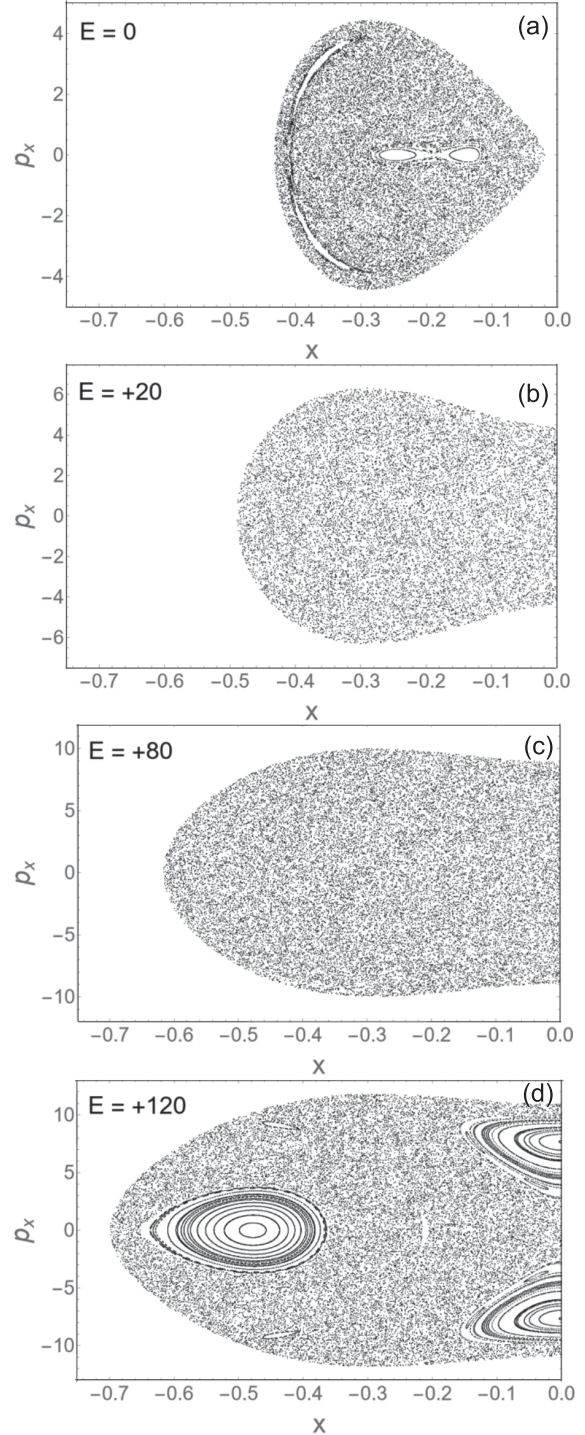


FIG. 6. Surfaces of section (p_x versus x plotted each time $z = 0$ for $p_z > 0$) for energies (a) $E = 0$, (b) $E = +20$, and (c) $E = +80$, and (d) $E = +120$.

quantum states for particles confined to the honeycomb optical lattice.

IV. QUANTUM DYNAMICS OF THE HONEYCOMB OPTICAL LATTICE

The unit cell of the quantum honeycomb lattice is shown in Fig. 7. The quantum unit cell is larger than the classical

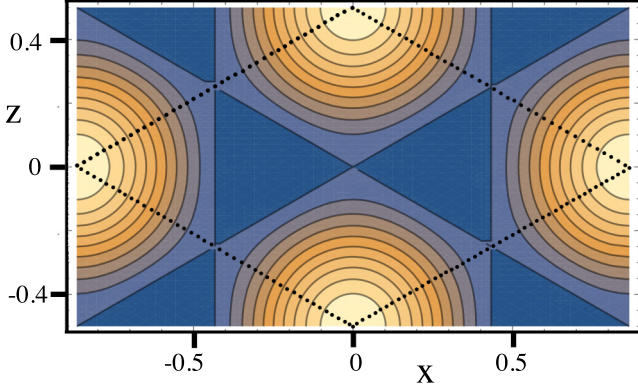


FIG. 7. The unit cell for the quantum dynamics is enclosed by the dark dotted lines.

unit cell because in honeycomb materials, such as graphene, the electrons attached to the carbon atoms that form the potential wells for the electrons have different spin and bonding orientations [10].

The primitive vectors for the graphene lattice, in dimensionless units, are $\mathbf{a}_1 = \frac{\sqrt{3}}{2}\hat{e}_x + \frac{1}{2}\hat{e}_z$ and $\mathbf{a}_2 = \frac{\sqrt{3}}{2}\hat{e}_x - \frac{1}{2}\hat{e}_z$. The unit cell has an area of $\Omega = \frac{\sqrt{3}}{2}$. The reciprocal lattice vectors \mathbf{b}_1 and \mathbf{b}_2 are defined $\mathbf{b}_1 = \frac{2\pi}{\sqrt{3}}\hat{e}_x + 2\pi\hat{e}_z$ and $\mathbf{b}_2 = \frac{2\pi}{\sqrt{3}}\hat{e}_x - 2\pi\hat{e}_z$ (see Fig. 8).

The ν th energy eigenstate of the unit cell has the form

$$u_\nu(\mathbf{r}) = \frac{1}{\sqrt{\Omega}} \sum_{n_1, n_2=-\infty}^{\infty} A_{n_1, n_2}(\nu) e^{i(n_1\mathbf{b}_1 + n_2\mathbf{b}_2) \cdot \mathbf{r}}. \quad (13)$$

A Bloch state, with wave vector \mathbf{k} , can be written

$$\psi_{\nu, \mathbf{k}}(\mathbf{r}) = e^{i\mathbf{k} \cdot \mathbf{r}} u_{\nu, \mathbf{k}}(\mathbf{r}). \quad (14)$$

Note that $u_{\nu, \mathbf{k}}(\mathbf{r}) = u_{\nu, \mathbf{k}}(\mathbf{r} + \mathbf{R})$, where \mathbf{R} is some combination of the lattice vectors \mathbf{a}_1 and \mathbf{a}_2 . The Bloch states then take the form

$$\psi_{\nu, \mathbf{k}}(\mathbf{r}) = \frac{1}{\sqrt{\Omega}} e^{i\mathbf{k} \cdot \mathbf{r}} \sum_{n_1, n_2=-\infty}^{\infty} A_{n_1, n_2}(\nu, \mathbf{k}) e^{i(n_1 + n_2)\frac{2\pi}{\sqrt{3}}x} e^{i(n_1 - n_2)2\pi z}. \quad (15)$$

The energy bands are given by the eigenvalue equation

$$\hat{H}^{(0)} \psi_{\nu, \mathbf{k}}(\mathbf{r}) = E_\nu^0(\mathbf{k}) \psi_{\nu, \mathbf{k}}(\mathbf{r}). \quad (16)$$

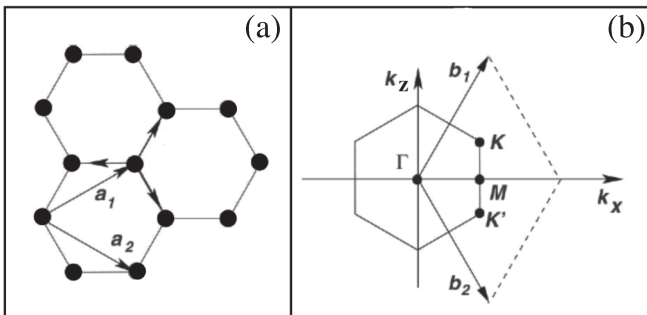


FIG. 8. (a) The primitive vectors \mathbf{a}_1 and \mathbf{a}_2 . (b) The reciprocal lattice vectors \mathbf{b}_1 and \mathbf{b}_2 .

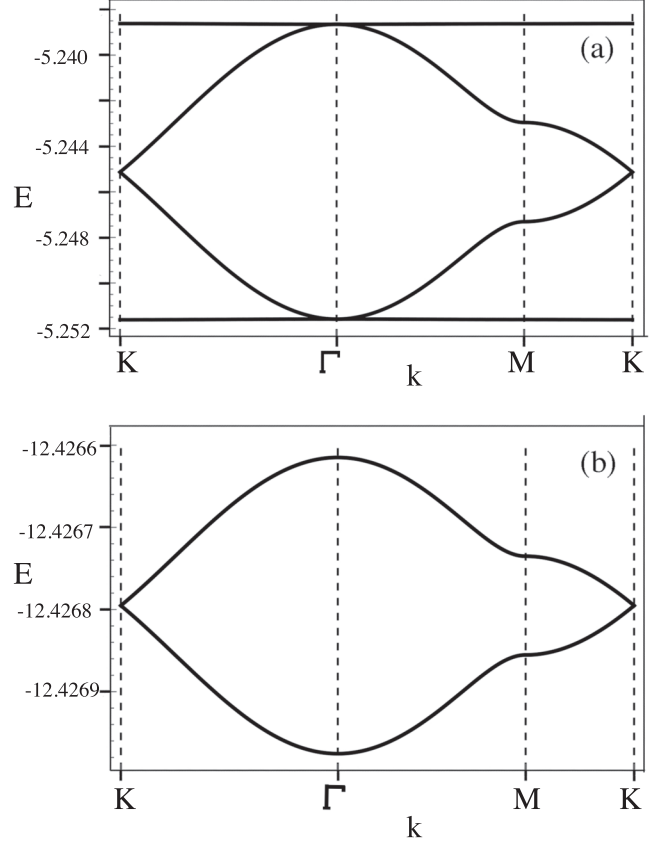


FIG. 9. The energy bands for energies $E < 0$. (a) For the lower-energy bands $-12.4269 \leq E \leq -12.4266$ (b) For the higher-energy bands $-5.238 \leq E \leq -5.252$.

The high-symmetry points of the honeycomb lattice, Γ , K , M , are given by $K = \frac{2}{3}\mathbf{b}_1 + \frac{1}{3}\mathbf{b}_2$, $\Gamma = 0$, and $M = \frac{1}{2}\mathbf{b}_1 + \frac{1}{2}\mathbf{b}_2$. The lattice vectors directed along the lines between the high-symmetry lines of the lattice often play a special role. For example, the wave vector which is directed from the Γ point to the K point is $\mathbf{k}_{\Gamma, K} = k(\frac{2\pi}{\sqrt{3}}\hat{e}_x + \frac{2\pi}{3}\hat{e}_y)$, where $0 \leq k \leq 1$ varies the length of the vector from $\mathbf{k}_{\Gamma, K} = \mathbf{0}$ to $\mathbf{k}_{\Gamma, K} = (\frac{2\pi}{\sqrt{3}}\hat{e}_x + \frac{2\pi}{3}\hat{e}_y)$.

Band structure along the symmetry lines

In Fig. 9, we plot the energy bands for the honeycomb optical lattice for energies $-20 < E < 0$. There are six bands for $E < 0$. The lowest two bands (for energies $-12.4269 \leq E \leq -12.4266$) are exactly what is expected in honeycomb-type lattices. These lowest-energy bands become degenerate at the K -points (the Dirac points). There are four bands at higher energy (for energies $-5.238 \leq E \leq -5.252$), two of which are completely flat. These higher-energy bands also have Dirac points.

In Figs. 10 and 11, we plot the energy bands for the honeycomb optical lattice for energies $E_{\text{tot}} > 0$. For all the cases shown, the bands have Dirac points. The signatures of chaos, which appear as avoided crossings between the bands, begin to become evident for energies $E_{\text{tot}} > 13.5$, but become common for energies above $E_{\text{tot}} = 24$. The apparent repulsion (avoided crossings) between different bands is a signature of

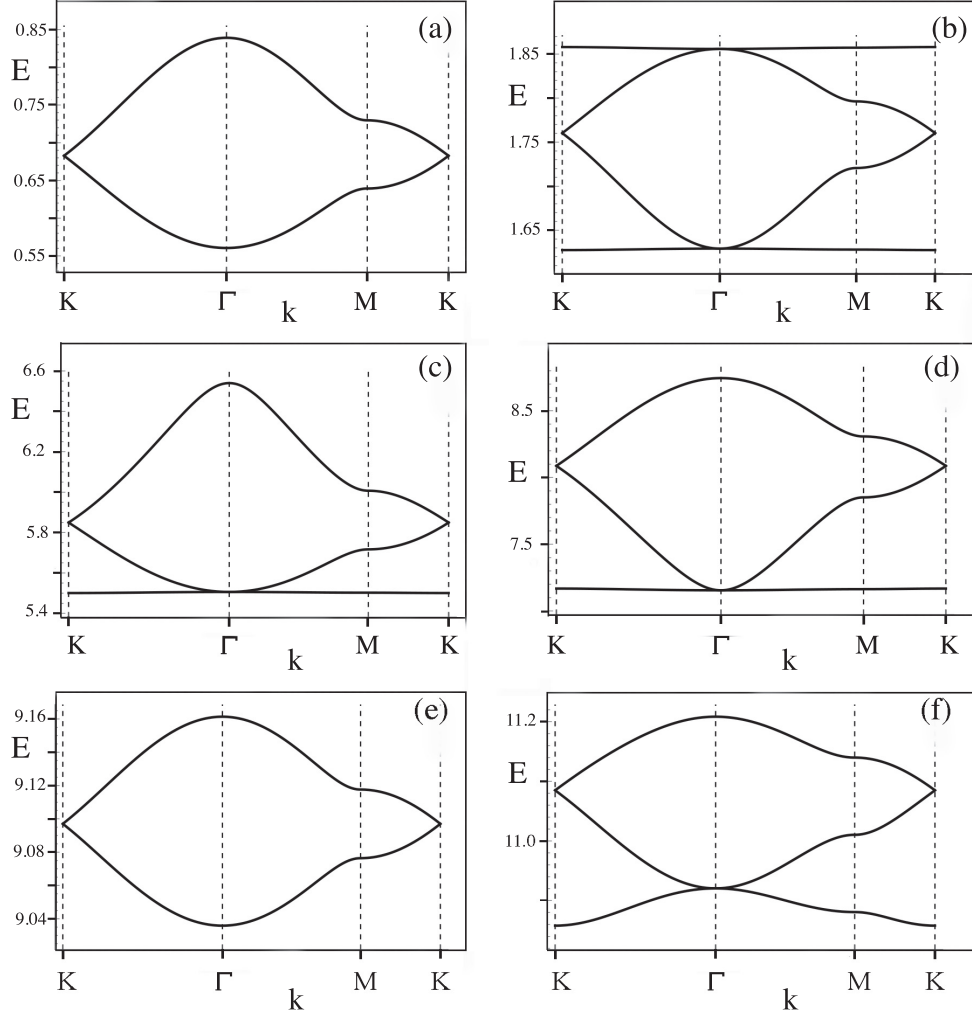


FIG. 10. The energy bands for energies $0 < E < 12$. The bands occur for energy intervals (a) $0.55 < E < 0.85$, (b) $1.60 < E < 1.90$, (c) $5.4 < E < 6.6$, (d) $7.0 < E < 9.0$, (e) $9.0 < E < 9.16$, and (f) $10.8 < E < 11.2$. In all cases, the bands have a Dirac point.

underlying chaos and causes mixing of the probability distributions associated with the various Bloch states involved in the avoided crossings [30,31].

V. CONCLUSIONS

Optical lattices provide a means to explore a number of quantum phenomena that cannot be easily explored in condensed matter systems. Their geometry is easily changed and controlled. They can accommodate both ultracold boson and fermion alkali gases. The honeycomb optical lattice is particularly interesting because of the profusion of Dirac points in the energy band structure. Ultracold atoms confined to optical lattices can act as analog quantum simulators because it is possible to track individual atoms [1,2]. They provide a means to study mechanisms for thermalization of isolated quantum systems, and to study the influence of the spatial structure of the lattice on the thermalization process.

APPENDIX A: OPTICAL LATTICE EFFECTIVE HAMILTONIAN

The Hamiltonian for the alkali atoms in dipole interaction with a y -polarized electric field can be written $H =$

$H_{\text{atom}} + H_{\text{int}}$, where

$$H_{\text{atom}} = \hbar\omega_{\text{at}}|e\rangle\langle e| + \frac{1}{2m}(p_x^2 + p_z^2)(|e\rangle\langle e| + |g\rangle\langle g|), \quad (\text{A1})$$

and

$$H_{\text{int}} = -dE_y(x, z, t)(|e\rangle\langle g| + |g\rangle\langle e|). \quad (\text{A2})$$

Here $\hbar\omega_{\text{at}}$ is the spacing of the two atomic energy levels, p_x (p_z) is the atomic momentum operator in the x (z) direction, and $d \equiv \langle e|\hat{d}_y|g\rangle = \langle g|\hat{d}_y|e\rangle$ is the field-induced dipole matrix element coupling the ground state $|g\rangle$ to the excited state $|e\rangle$ [17,18]. We consider an electric field that has the form

$$E_y(x, z, t) = E_o[\cos(\omega_L t) + \cos(k_L U + \omega_L t) + \cos(k_L V + \omega_L t)], \quad (\text{A3})$$

where $U = (z + \frac{x}{\sqrt{3}})$ and $V = (z - \frac{x}{\sqrt{3}})$. We can now rewrite this in the form

$$E_y(x, z, t) = \mathcal{E}(x, z)e^{+i\omega_L t} + \mathcal{E}^*(x, z)e^{-i\omega_L t}. \quad (\text{A4})$$

A time-dependent unitary transformation of the Schrödinger equation, given by $U = \exp[i\omega_L t|e\rangle\langle e|]$, and $H \rightarrow \mathcal{U}H\mathcal{U}^\dagger + i\hbar\frac{\partial\mathcal{U}}{\partial t}\mathcal{U}^\dagger$, transforms the Hamiltonian to the

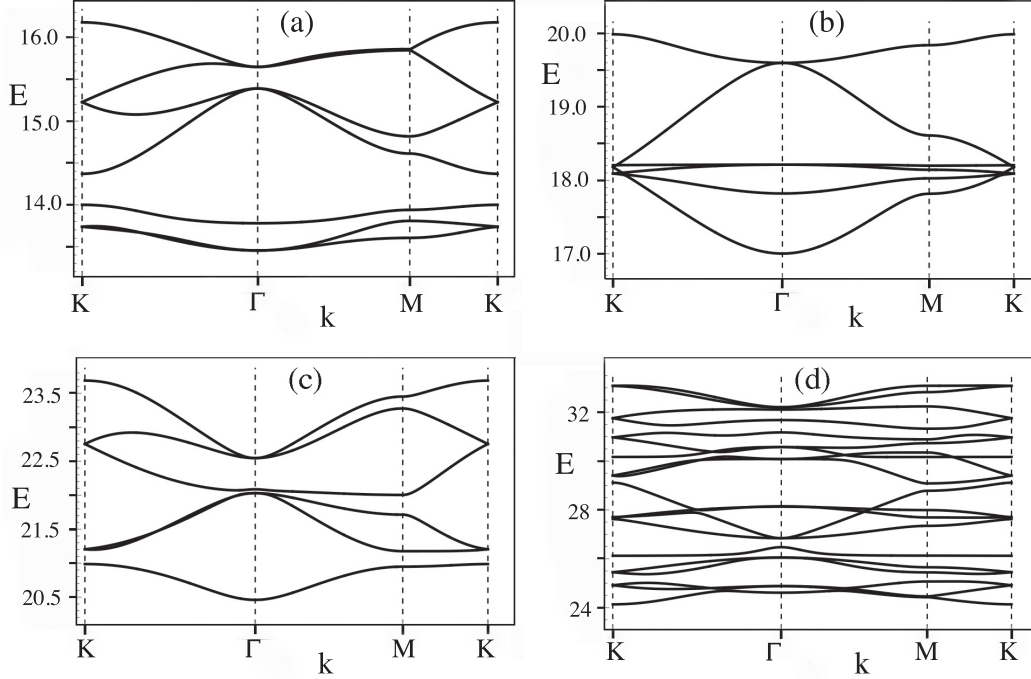


FIG. 11. The energy bands for energies $12 < E < 40$. The bands occur for energy intervals (a) $13.2 < E < 16.3$, (b) $16.7 < E < 20.0$, (c) $20.0 < E < 23.8$, and (d) $23.8 < E < 33$. In all cases the bands have at least one Dirac point.

rotating frame of the laser and gives

$$H = \hbar\Delta|e\rangle\langle e| + \frac{(p_x^2 + p_z^2)}{2m}(|e\rangle\langle e| + |g\rangle\langle g|) - d[\mathcal{E}(x, z, t)|e\rangle\langle g| + \mathcal{E}^*(x, z, t)|g\rangle\langle e|], \quad (\text{A5})$$

where $\Delta = \omega_{\text{at}} - \omega_L$ is the detuning of the reference radiation frequency from the atomic transition, and we have neglected rapidly oscillating terms containing $e^{\pm i\omega_L t}$.

Writing an arbitrary state $|\psi\rangle = \psi_g(x, t)|g\rangle + \psi_e(x, t)|e\rangle$, the Schrödinger equation can be written

$$i\hbar \frac{\partial \psi_g}{\partial t} = -\frac{\hbar^2}{2m} \left(\frac{\partial^2}{\partial x^2} + \frac{\partial^2}{\partial z^2} \right) \psi_g - d\mathcal{E}^*(x, z, t)\psi_e, \quad (\text{A6})$$

$$i\hbar \frac{\partial \psi_e}{\partial t} = -d\mathcal{E}(x, z, t)\psi_g + \left[\hbar\Delta - \frac{\hbar^2}{2m} \left(\frac{\partial^2}{\partial x^2} + \frac{\partial^2}{\partial z^2} \right) \right] \psi_e. \quad (\text{A7})$$

Adiabatic elimination of the excited state is performed by assuming that the detuning of the laser Δ is large enough to allow us to neglect the time and space derivatives of the excited state. Thus, atoms prepared in the ground state will remain there and we are left with an *effective Hamiltonian* for their evolution:

$$i\hbar \frac{\partial \psi_g}{\partial t} = H_{\text{eff}} \psi_g; \quad H_{\text{eff}} = \frac{p_x^2}{2m} + \frac{p_z^2}{2m} - \frac{d^2 |\mathcal{E}(x, z, t)|^2}{\hbar\Delta}, \quad (\text{A8})$$

where

$$|\mathcal{E}(x, z, t)|^2 = \frac{3}{4}E_o^2 + \frac{E_o^2}{2} \cos[k_L U] + \frac{E_o^2}{2} \cos[k_L V] + \frac{E_o^2}{2} \cos[k_L(U - V)]. \quad (\text{A9})$$

APPENDIX B: NUMBERS FOR ULTRACOLD CESIUM ATOMS

A series of past experiments [32–35] studied the behavior of cesium atoms in an optical lattice with one space dimension. Cesium atoms have a (field-induced) dipole moment $d = 2.2 \times 10^{-29}$ cm and an atomic transition frequency $\omega_{\text{at}} = 5 \times 10^8$ Hz [32]. The laser wavelength was $\lambda_L = 8.52 \times 10^{-5}$ cm [32], so the wave vector was $k_L = \frac{2\pi}{\lambda_L} = 7.37 \times 10^4$ rad/cm. The laser frequency was $\omega_L = k_L c = 2.2 \times 10^{15}$ rad/s.

When the cesium atoms interact with the laser field that forms the honeycomb optical lattice, there is a recoil and the atoms change momentum in the z direction by the discrete amount $\Delta p_z = 2\hbar k_L$, and in the x direction by $\Delta p_x = 2\hbar k_L / \sqrt{3}$. The atomic energies change by the recoil energy $\hbar\omega_R = \frac{\hbar^2 k_L^2}{2m} = 1.4 \times 10^{-23}$ erg in the z direction, and by $\frac{1}{3}\hbar\omega_R$ in the x direction.

The depth of the honeycomb potential well can be changed by changing the strength of the electric field E_o and intensity of the radiation. In these experiments $\frac{d^2 |E_o|^2}{2\hbar\Delta} = (5.14 \times 10^{-24} \text{ erg}) \alpha$, where α is a dimensionless parameter (of order one) that can be varied by changing the intensity of the radiation field. Thus, the dimensionless interaction strength U_o is $U_o = \frac{d^2 |E_o|^2}{2\hbar\Delta} \frac{2m}{\hbar^2 k_L^2} = \frac{(5.14 \times 10^{-24} \text{ erg}) \alpha}{1.4 \times 10^{-23} \text{ erg}} = 0.367\alpha$.

- [1] C. Gross and I. Bloch, *Science* **357**, 995 (2017).
- [2] F. Schäfer, T. Fukuhara, S. Sugawa, Y. Takasu, and Y. Takahashi, *Nat. Rev. Phys.* **2**, 411 (2020).
- [3] M. Srednicki, *Phys. Rev. E* **50**, 888 (1994).
- [4] Y. G. Sinai, *Russ. Math. Surv.* **25**, 137 (1970).
- [5] L. Bunimovich, *Scholarpedia* **2**, 1813 (2007).
- [6] N. Friedman, A. Kaplan, D. Carasso, and N. Davidson, *Phys. Rev. Lett.* **86**, 1518 (2001).
- [7] L. Ermann, E. Vergini, and D. L. Shepelyansky, *Europhys. Lett.* **111**, 50009 (2015).
- [8] L. Ermann, E. Vergini, and D. L. Shepelyansky, *Phys. Rev. A* **94**, 013618 (2016).
- [9] L. Tarruell, D. Greif, T. Uehlinger, G. Jotzu, and T. Esslinger, *Nature (London)* **483**, 302 (2012).
- [10] R. Saito, G. Dresselhaus, and M. S. Dresselhaus, *Physical Properties of Carbon Nanotubes* (Imperial College Press, London, 1998).
- [11] M. I. Katsnelson, *Graphene: Carbon in Two Dimensions* (Cambridge University Press, Cambridge, 2012).
- [12] F. D. M. Haldane and S. Raghu, *Phys. Rev. Lett.* **100**, 013904 (2008).
- [13] R. A. Sepkhanov, Y. B. Bazaliy, and C. W. J. Beenakker, *Phys. Rev. A* **75**, 063813 (2007).
- [14] R. A. Sepkhanov, J. Nilsson, and C. W. J. Beenakker, *Phys. Rev. B* **78**, 045122 (2008).
- [15] K. L. Lee, B. Gremaud, R. Han, B.-G. Englert, and C. Miniatura, *Phys. Rev. A* **80**, 043411 (2009).
- [16] M. D. Porter and L. E. Reichl, *Phys. Rev. E* **93**, 012204 (2016).
- [17] R. Graham, M. Schlautmann, and P. Zoller, *Phys. Rev. A* **45**, R19 (1992).
- [18] B. P. Holder and L. E. Reichl, *Phys. Rev. A* **76**, 013420 (2007).
- [19] B. Eckhardt, *J. Phys. A: Math. Gen.* **20**, 5971 (1987).
- [20] P. Gaspard and S. A. Rice, *J. Chem. Phys.* **90**, 2225 (1989).
- [21] C. Jung and P. H. Richter, *J. Phys. A: Math. Gen.* **23**, 2847 (1990).
- [22] L. E. Reichl, *The Transition to Chaos*, 3rd ed. (Springer Nature Switzerland AG, Cham, 2021).
- [23] M. Born, *The Mechanics of the Atom* (Frederick Ungar, New York, 1960).
- [24] G. H. Walker and J. Ford, *Phys. Rev.* **188**, 416 (1969).
- [25] V. I. Arnold, *Sov. Math. Dokl.* **5**, 581 (1964); [Reprinted in R. S. MacKay and J. D. Meiss, *Hamiltonian Dynamical Systems* (Adam Higler, Bristol, 1987)].
- [26] Y. Boretz and L. E. Reichl, *Phys. Rev. E* **93**, 032214 (2016).
- [27] A. N. Kolmogorov and D. Akad. Nauk SSSR **98**, 527 (1954); [English translation in R. Abraham, *Foundations of Mechanics* (W. A. Benjamin, New York, 1967), Appendix D].
- [28] V. I. Arnol'd, *Russ. Math. Surv.* **18**, 9 (1963).
- [29] J. Moser, *Comm. Pure Appl. Math.* **11**, 81 (1958).
- [30] M. D. Porter, A. D. Barr, A. R. Barr, and L. E. Reichl, *Phys. Rev. E* **95**, 052213 (2017).
- [31] A. D. Barr, A. R. Barr, M. D. Porter, and L. E. Reichl, *Chaos* **27**, 104604 (2017).
- [32] D. A. Steck, V. Milner, W. H. Oskay, and M. G. Raizen, *Phys. Rev. E* **62**, 3461 (2000).
- [33] D. A. Steck, W. H. Oskay, and M. G. Raizen, *Science* **293**, 274 (2001).
- [34] D. A. Steck, W. H. Oskay, and M. G. Raizen, *Phys. Rev. Lett.* **88**, 120406 (2002).
- [35] R. Luter and L. E. Reichl, *Phys. Rev. A* **66**, 053615 (2002).

Correction: The second author's name was presented incorrectly and has been fixed.